Journal of Organometallic Chemistry 694 (2009) 1623–1631

Contents lists available at ScienceDirect

Journal of Organometallic Chemistry

journal homepage: www.elsevier.com/locate/jorganchem

Group 4 *ansa*-metallocenes derived from *o*-carborane and their luminescent properties

Chang Hwan Shin, Yonggyu Han, Min Hyung Lee *, Youngkyu Do *

Department of Chemistry, School of Molecular Science BK-21, KAIST, Daejeon 305-701, Republic of Korea

ARTICLE INFO

Article history:
Received 23 September 2008
Received in revised form 24 December 2008
Accepted 24 December 2008
Available online 4 January 2009

Keywords:
o-Carborane
Group 4 metallocene
Mechanoluminescence
Electroluminescence
Electron-transporting

ABSTRACT

Luminescent group 4 complexes derived from *o*-carborane, M(η^5:η^1-CpCMe$_2$CB$_{10}$H$_{10}$C)$_2$ (M = Ti; **1**, Zr; **2**, Hf; **3**) and Me$_2$Si(η^5-Ind)[η^5:η^1-Cp-3-(CMe$_2$CB$_{10}$H$_{10}$C)]ZrCl (**4**) were explored. While the Ti complex **1** possessing C_2 molecular symmetry shows non-centrosymmetry in the unit cell as identically observed in **2** and **3**, the double-*ansa* Zr complex **4** crystallizes in centrosymmetric $P2_1/n$ space group despite its C_1 molecular symmetry. The non-centrosymmetric crystals of **2** and **3** exhibit blue mechanoluminescence similar to their solution and solid state photoluminescence. In contrast, **1** is lacking mechanoluminescence in crystal and shows much weaker emission than other congeners in solution. The electroluminescence devices based on **2** or **3** doped poly(*N*-vinylcarbazole) (PVK) as an emitting layer display green electroluminescence, which turned out to be originated from the exciplexes formed between the complex and PVK host. Although the double *ansa*-Zr complex **4** does not show mechanoluminescence owing to the centrosymmetric nature, it exhibits good electron-transporting properties when incorporated into the electron-transporting layer of Alq$_3$-based OLEDs.

1. Introduction

Luminescent metal complexes have been extensively investigated owing to their potential applications in various areas such as organic light-emitting diodes [1], photovoltaic devices [2], and sensory systems [3]. In particular, the molecular system with multi-luminescent properties would be also intriguing since the strategy of one-source-multi-application can be implemented. Nonetheless, the example of such molecular system is limited to dissymmetric Hf(η^5:η^1-CpCMe$_2$CB$_{10}$H$_{10}$C)$_2$ (**3**) that constitutes unique organometallic system showing various luminescent properties of photo-, mechano- and electroluminescence [4]. The isopropylidene-bridged cyclopentadienyl *o*-carboranyl ligand HCpCMe$_2$CB$_{10}$H$_{10}$CH (**I**) [5] is considered to play a key role in the manifestation of multi-luminescent properties of the foregoing Hf system since **I** not only contains potentially luminophoric [6] *o*-carborane framework but also easily endows a molecule with chirality, a prerequisite to the non-centrosymmetric crystal system that in turn a prerequisite to mechanoluminescence [7]. Thus, our efforts to develop the molecular system with multi-luminescent properties, reported in this article, have been directed toward the investigation of luminescent properties of group 4 congener set of **I** (**1**–**3**). In addition, the synthesis of a new double *ansa*-type ligand Me$_2$Si(HInd)(HCp-3-(CMe$_2$CB$_{10}$H$_{10}$CH)) (**II**) by introducing an indenyl-silyl unit to **I** and the chemistry of zirconium complex of **II** (**4**) are also reported here since such a double *ansa*-complex possesses C_1 molecular symmetry and thereby is potentially anticipated to exhibit interesting luminescent properties as observed in the dissymmetric **3**.

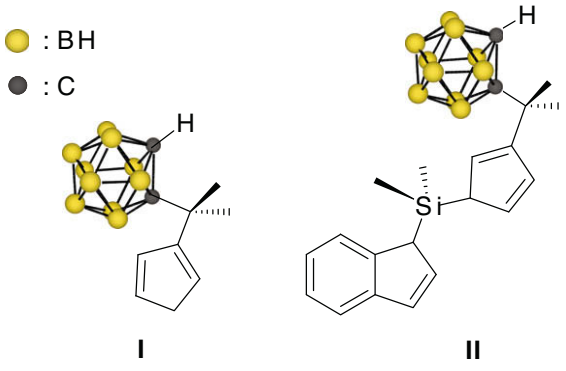

2. Results and discussion

2.1. Synthesis and characterization

Orange solid titanium complex **1** was prepared according to a procedure analogous to its Zr (**2**) [5] and Hf (**3**) [4] congeners (Fig. 1). Synthetic routes to the ligand **II** and its Zr complex Me$_2$Si(η^5-Ind)[η^5:η^1-Cp-3-(CMe$_2$CB$_{10}$H$_{10}$C)]ZrCl (**4**) are depicted in

* Corresponding authors.
E-mail addresses: lmh74@kaist.ac.kr (M.H. Lee), ykdo@kaist.ac.kr (Y. Do).

0022-328X/$ - see front matter © 2009 Elsevier B.V. All rights reserved.
doi:10.1016/j.jorganchem.2008.12.062

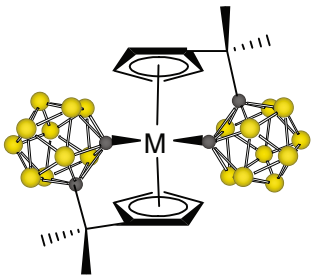

Fig. 1. Dissymmetric group 4 complexes derived from *o*-carborane.

Scheme 1. Potentially heptadentate double-*ansa*-type ligand **II** was readily prepared as pale yellow oil from the reaction of mono-lithiated product of **I** with 1-(chlorodimethylsilyl)indene [8]. While the direct metallation reaction from the trilithium salt of **II** with $ZrCl_4$ failed to give the desired zirconium complex, the treatment of **II** with $Zr(NMe_2)_4$ in refluxing hexanes produces $Me_2Si(\eta^5\text{-Ind})[\eta^5{:}\eta^1\text{-Cp-3-}(CMe_2CB_{10}H_{10}C)]ZrNMe_2$ that in turn affords **4** in high yield in the presence of excess Me_3SiCl. The identity of **1** and **4** has been confirmed by NMR spectroscopy, elemental analysis, and X-ray diffraction study. In both complexes, the ^1H NMR spectra exhibit chemically inequivalent four and three proton resonances for the cyclopentadienyl groups, respectively. The well-resolved methyl proton resonances of both the $SiMe_2$ and CMe_2 bridging groups in **4** are in good agreement with the expected C_1 molecular symmetry of **4**. The ^{11}B NMR spectra of both complexes which feature four signals with the intensity ratio of 2:2:4:2 derived from the *o*-carborane cage are also comparable to those of the reported *o*-carboranyl metallocene complexes [4,5,9].

The X-ray crystal structure of **1** shown in Fig. 2 is similar to its zirconium (**2**) and hafnium (**3**) congeners reported previously, exhibiting a distorted tetrahedral arrangement of the ligands around the Ti center with C_2 symmetry. Although the Ti–Cp distances and Cp–Ti–Cp′ angles for **1** are in good agreement with those observed in the usual titanocenes [10], the smaller size of Ti atom results in the slight variations in the bond distances and angles compared to those of **2** and **3** despite the overall structural similarity; the shorter Ti–Cp(centroid) distances of 2.0551(15) Å (C4–C8 ring) and 2.0679(14) Å (C4′–C8′ ring) and Ti–caboranyl carbon distances of 2.308(7) Å (Ti–C1) and 2.308(10) Å (Ti–C1′) in **1** than those of **2** (2.192 Å for Zr–Cp(centroid) and avg. 2.37 Å for Zr–C1) and **3** (2.178 Å for Hf–Cp(centroid) and avg. 2.34 Å for Hf–C1) and the larger Cp–Ti–Cp′ angle of 129.10° (**1**) than 128.70° (**2**) and 127.91° (**3**) [4,5].

According to the molecular structure of **4** displayed in Fig. 3, it can be seen that the zirconium atom bonds with Cp and indenyl rings in a η^5 bonding fashion and with the *o*-carboranyl cage in a η^1 fashion, exhibiting a double *ansa*-metallocene structure. The overall molecular structure possesses C_1 molecular symmetry. The Zr–Cp(centroid) and Zr–Ind(centroid) distances of 2.1796(6) Å and 2.222(2) Å, respectively, and the Cp(centroid)–Zr–Ind(centroid) and Cp(C1)–Si–Ind(C11) angles of 127.33(9)° and 94.4(2)°, respectively, are comparable to those of the $Me_2Si(\eta^5\text{-Ind})(\eta^5\text{-Cp})ZrCl_2$ complex [11]. The Zr–carboranyl carbon distance of 2.361(5) Å is also in the very similar range observed for **2** (avg. 2.37 Å) [5] and the related *o*-carboranyl zirconocene complexes (2.31–2.36 Å) [9]. While the Ti complex **1** which possesses C_2 symmetry belongs to non-centrosymmetric space group $P2_1$ as identically observed in **2** and **3**, the double-*ansa* Zr complex **4** crystallizes in centrosymmetric $P2_1/n$ space group with the inversion center in the unit cell despite its C_1 molecular symmetry.

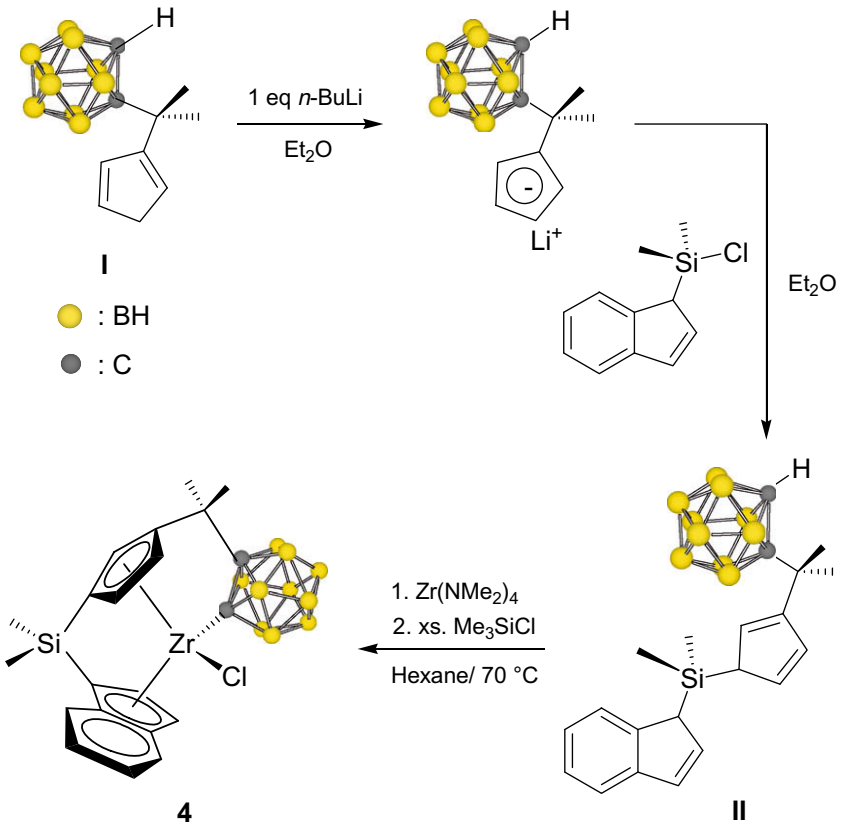

Scheme 1. Synthetic route to double *ansa*-zirconocene complex **4**.

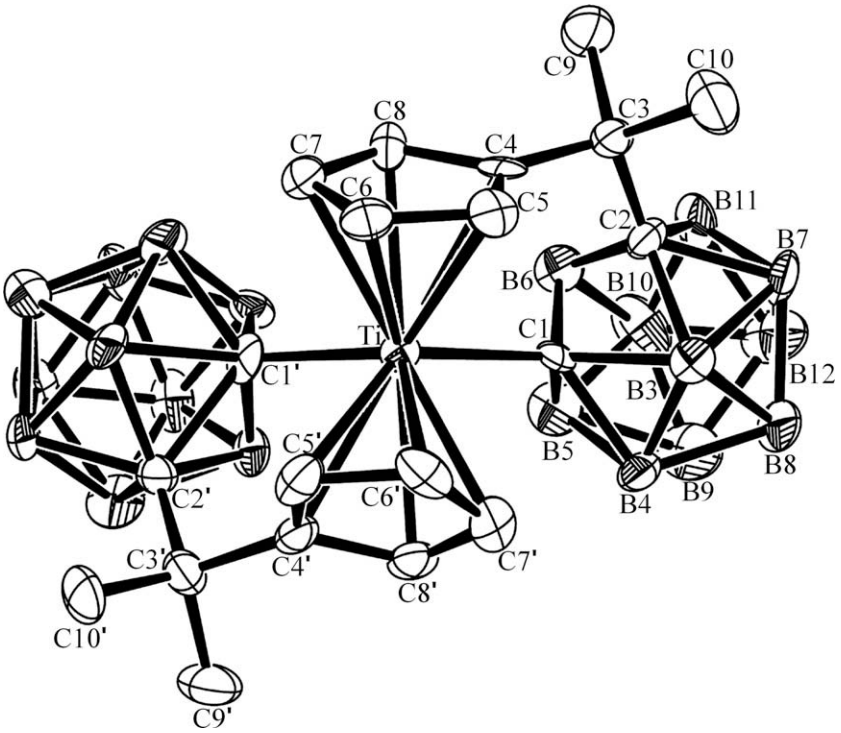

Fig. 2. Molecular structure of **1** (50% thermal ellipsoid). Hydrogen atoms are omitted for clarity. Selected bond distances (Å) and angles (°): Ti–C1 2.308(7), Ti–C1′ 2.308(10), Ti–C4 2.419(4), Ti–C4′ 2.406(4), Ti–C5 2.395(4), Ti–C5′ 2.399(4), Ti–C6 2.357(4), Ti–C6′ 2.387(4), Ti–C7 2.357(4), Ti–C7′ 2.386(4), Ti–C8 2.395(4), Ti–C8′ 2.397(4), C1–Ti–C1′ 106.4(3), Ti–C1–C2 117.0(5), Ti–C1′–C2′ 118.7(6), C2–C3–C4 109.7(4), C2′–C3′–C4′ 106.2(4).

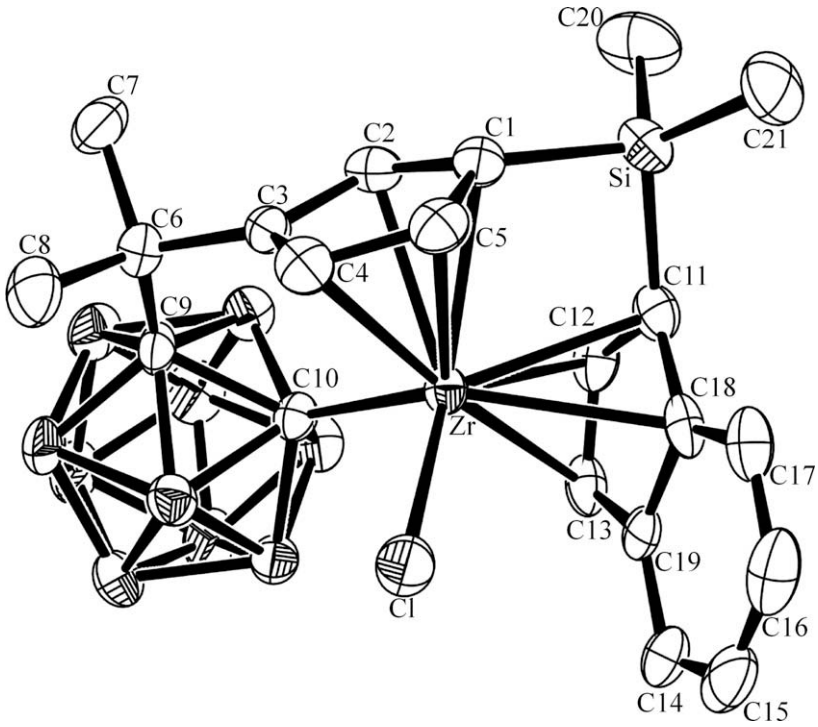

Fig. 3. Molecular structure of **4** (50% thermal ellipsoid). Hydrogen atoms are omitted for clarity. Selected bond distances (Å) and angles (°): Zr–C1 2.477(5), Zr–C2 2.474(5), Zr–C3 2.531(5), Zr–C4 2.512(5), Zr–C5 2.455(5), Zr–C10 2.361(5), Zr–C11 2.465(5), Zr–C12 2.458(5), Zr–C13 2.560(5), Zr–C18 2.529(5), Zr–C19 2.641(5), Zr–Cl 2.4180(14), C9–C10 1.703(7), Zr–C10–C9 116.9(3), C3–C6–C9 109.6(4), C1–Si–C11 94.4(2).

2.2. Luminescent properties of dissymmetric ***1–3***

2.2.1. Mechano- and photoluminescence in solid state

Since dissymmetric complexes **1–3** constitute non-centrosymmetric crystal system which may yield mechanoluminescence (ML) [7], the ML measurements were carried out and the ML spectra are displayed in Fig. 4. While the Zr and Hf complexes **2** and **3** exhibit ML maxima at 459 and 435 nm, respectively, the Ti complex **1** is lacking ML. The ML spectra of **2** and **3** are different from the molecular nitrogen discharge spectrum [12] but resemble their

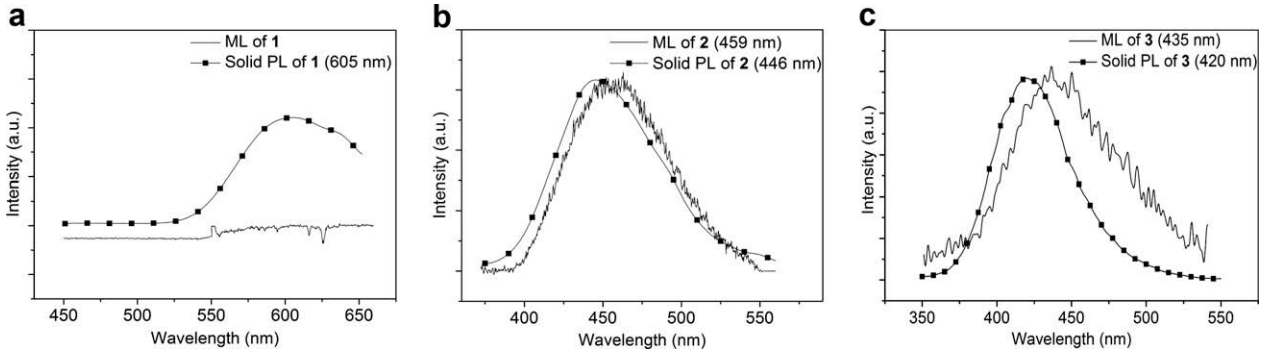

Fig. 4. Solid PL and ML spectra of (a) **1**, (b) **2**, and (c) **3**.

photoluminescence (PL) spectra in the solid state as shown in Fig. 4. Thus, the origin of the ML for **2** and **3** can be ascribed to the direct excitation of the crystal molecules rather than the discharge of adjacent gas molecules such as N_2.

It is also interesting to note that the ML maxima of **2** and **3** are red-shifted from their PL peaks by 13 and 15 nm, respectively. Several origins have been suggested to explain such spectral differences between ML and PL: self-absorption of ML light, pressure-induced changes of the Franck–Condon factors, and generation of different excited-states by fracture-induced symmetry changes in applying strong pressures [13,14]. The self-absorption of ML light is not likely to occur in **2** and **3** as judged by their large Stokes shift in solution (~100 nm) (Fig. 5). It is also expected that the pressure-induced changes of Franck–Condon factors could be small in **2** and **3** presumably due to the long emission lifetime (~μs, Table 2) compared with the very short duration of applying pressures (~ps) [13].

Therefore, it seems that the red-shift of ML spectra in **2** and **3** is caused by generation of different excited-states by fracture-induced symmetry change. In contrast to **2** and **3**, the absence of ML in **1** might indicate that the emission can be easily quenched or not allowed because there is a marked difference between the band structure of the ground state and that of the excited state in **1** as supported by very large Stokes shift of about 200 nm for **1** in solution (Fig. 5).

2.2.2. Photophysical properties in solution

The absorption spectra of **1–3** exhibit low-energy absorption bands assignable to ligand-to-metal charge transfer (LMCT) transitions usually observed in the d^0 complexes (Fig. 5) [15]. While the absorption spectra of the white complexes **2** and **3** are similar to each other with the absorption maxima at 290 nm, the orange complex **1** features the overall red-shifted band with the peak maximum at 410 nm. Weak shoulders are also observed at the lower energy region around 319 nm and 311 nm for **2** and **3**, respectively.

All the carborane complexes are emissive in solution state at ambient condition (Table 2 and Fig. 5). The solution PL spectra of **1–3** are structureless with peak maxima at 602, 441 and 419 nm, respectively, and the emission energy follows the order of Hf > Zr > Ti. It is noteworthy that the solution PL maximum wave-

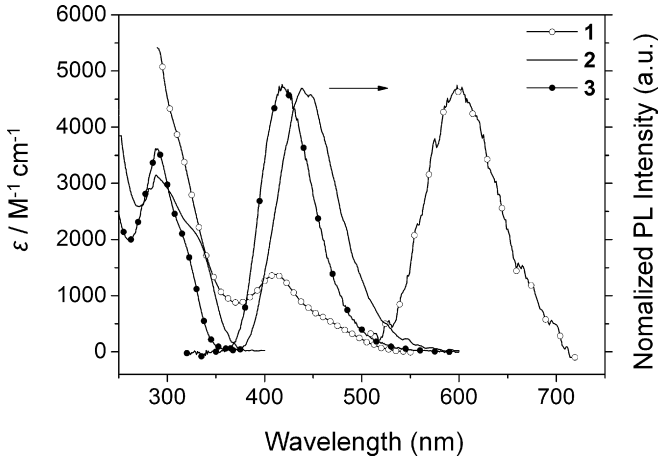

Fig. 5. UV–Vis absorption and emission spectra of **1–3** in THF.

Table 1
Crystallographic data and parameters for **1** and **4**.

Compound	**1**	**4**
Empirical formula	$C_{20}H_{40}B_{20}Ti$	$C_{21}H_{31}B_{10}ClSiZr$
Formula weight	544.62	546.32
T (K)	293	293
Wavelength (Å)	0.71073	0.71073
Crystal system	Monoclinic	Monoclinic
Space group	$P2_1$	$P2_1/n$
a (Å)	9.331(3)	7.9300(8)
b (Å)	9.6410(10)	22.693(2)
c (Å)	16.416(3)	14.4656(15)
α (°)	90	90
β (°)	103.24(2)	100.656(2)
γ (°)	90	90
V (Å^3)	1437.5(6)	2558.3(4)
Z	2	4
ρ_{calc} (g cm^3)	1.258	1.418
μ (mm^1)	0.313	0.592
F(000)	564	1112
Number of reflections measured	4621	9871
Number of reflections used (R_{int})	2547 (0.0922)	5630 (0.0731)
Goodness-of-fit on F^2	1.004	1.004
R_1[a], wR_2[b] ($I > 2\sigma(I)$)	0.0745, 0.1011	0.0683, 0.1323
ρ_{fin} (max/min) (e Å^3)	0.297/0.303	1.072/0.642

[a] $R_1 = \sum||F_o| - |F_c||/\sum|F_o|$.
[b] $wR_2 = [\sum[w(F_o^2 - F_c^2)^2]/\sum[w(F_o^2)^2]]^{1/2}$, where $w = 1/[\sigma^2(F_o^2) + (xP)^2 + yP]$, $P = (F_o^2 + 2F_c^2)/3$.

Table 2
Photophysical data of **1–3** in solution[a].

Compound	λ_{abs} (nm) (ε [mol^{1}cm^1])	λ_{em} (nm)	η_{PL}[b] (%)	τ (μs)
1	302 (4360), 410 (1380)	602	0.04	2.6
2	290 (3110), 319 (2310)	441	0.3	1.4
3	290 (3610), 311 (2290)	419	1.5	1.2

[a] ~10^{-4} M of THF (**1–3**) solutions at room temperature.
[b] λ_{exc} = 355 nm; PL quantum yields determined relative to 10^{-5} M quinine sulfate dihydrate in 1 N H_2SO_4 solution (η = 54.6%) at room temperature [17].

lengths are in good agreement with their solid-state PL maxima (Fig. 4). The PL quantum yields obtained at room temperature are in the increasing order of **1** << **2** < **3** from Φ = 0.04–1.5%. The very low quantum yield for **1** is in parallel with the previous finding that the excited states of titanocene complexes are unstable at room temperature [16]. The PL lifetime of ca. 1–3 μs at room temperature is also indicative of the LMCT phosphorescence as typically known in the Cp_2MCl_2 (M = Ti, Zr, Hf) complexes [15].

2.2.3. Electroluminescence and exciplex formation

The carborane complexes **2–3** were employed into electroluminescence (EL) devices as emitting materials by spin-casting method because they are not sublimable. The devices consist of ITO/PVK:**2** or **3**/Li:Al (5:95). PVK (poly(*N*-vinylcarbazole)) polymer which is widely used as a host of organic light emitting diodes (OLEDs) was chosen because of wide bandgap and hole-transporting property [18], and the blending concentration of **2** or **3** was varied from 0.5 to 5.0 wt.%. For the 3 wt.% blended system, the turn-on voltage was 16 V and the maximum brightness was 47 cd/m^2 at 30 V.

As shown in Fig. 6, **2** and **3** show green EL with the maximum wavelength at 562 nm and 537 nm, respectively, that is largely red-shifted with respect to their solution PL (Fig. 5). A weak shoulder at 446 nm is observed for the Hf complex **3**. The slightly red-shifted EL spectrum of **2** compared to that of **3** is similar with the trend in the solution PL spectra. In conjunction with the weak luminance, such a different feature between the EL and the solution PL spectra may suggest the possibility of exciplex emission [19]. To gain insight into the exciplex formation, the PL spectra of PVK films doped with 5 wt.% of **2** or **3** on quartz substrate were further examined. Besides the major blue emission at 409 nm, the green peaks appear at the lower energy region around 550 nm in each PL spectrum (Fig. 6), and the latter peaks are well matched with their EL peaks. While the lower energy PL peak of **2** is red-shifted with respect to that of **3**, as similarly observed in the EL spectra, the higher energy peaks of **2** and **3** are essentially identical in terms of shape and maximum wavelength, implying that the higher energy peaks are originated from the PVK host [18]. Interestingly, there are no observable peaks that are consistent with the solid-state PL maximum wavelengths of **2** and **3** (446 nm and 420 nm, respectively; Fig. 4). All these results thus indicate that the green emission in both EL and PL spectra can be ascribable to the exciplex formed between the carborane complex and PVK host.

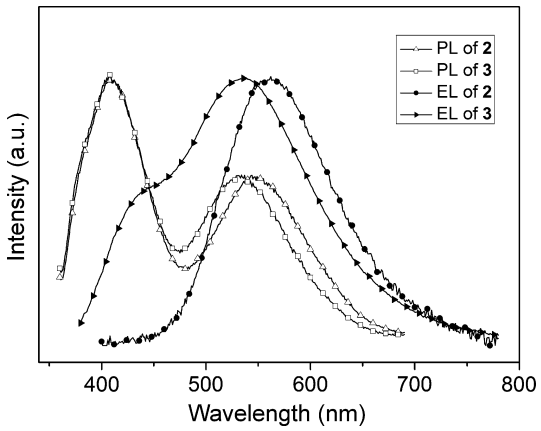

Fig. 6. EL spectra of **2** or **3**-based devices and PL spectra of **2** or **3**-doped PVK film.

The comparative PL studies of doped **2** in various hosts were performed to investigate the exciplex emission in more detail. The used hosts are illustrated in Fig. 7.

PVK polymer has aromatic side chains with amine moiety. Based on this structure, polymer hosts were chosen as follows; PF (polyfluorene) is blue-emitting polymer with aromatic main chains, PS (polystyrene) is non-emitting polymer with aromatic side chains, and PMMA (poly(methylmethacrylate)) is non-emitting polymer without aromatic side chains. Among them, the additional peak occurred only in PVK film as illustrated in Fig. 8. The PF film showed only PF emission, and the PS and PMMA films showed the identical emission with the solution PL of **2**. These results indicate the involvement of an amine moiety in the formation of new emission. Hence, organic amine hosts were further investigated to probe the effect of amine moiety. The selected organic compounds are EC (9-ethylcarbazole) and TPA (triphenylamine) that are blue-emitting. Since it is difficult to prepare films by only organic compounds, the blends of non-emitting PMMA polymer with the organics in the ratio of 7:3 were used. As shown in Fig. 8, the structured emission peak at around 400 nm from each organic host and another large peak in the green region were obtained, and the latter peak is very similar to that found in the PVK film. The Hf complex **3** gave similar results in the same experiments. From these results, it is confirmed that an exciplex is formed between N-containing host and the carborane complex. It could be thus suggested that the exciplex formation is favored by the interaction between

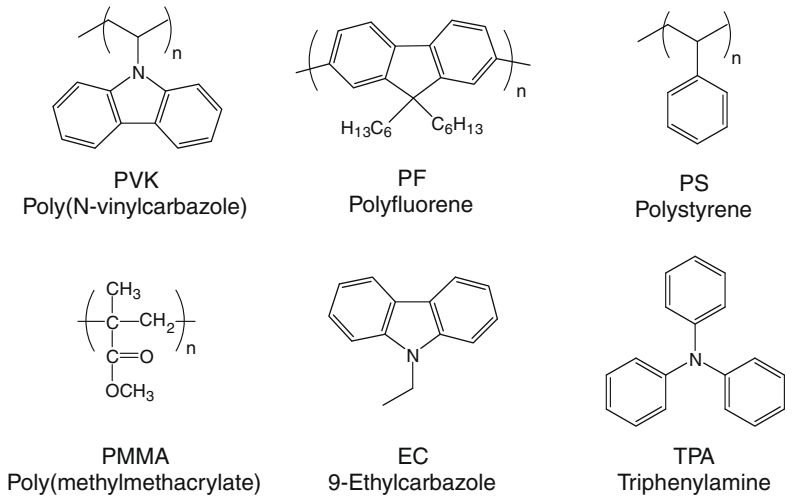

Fig. 7. Polymers and organic compounds used as hosts.

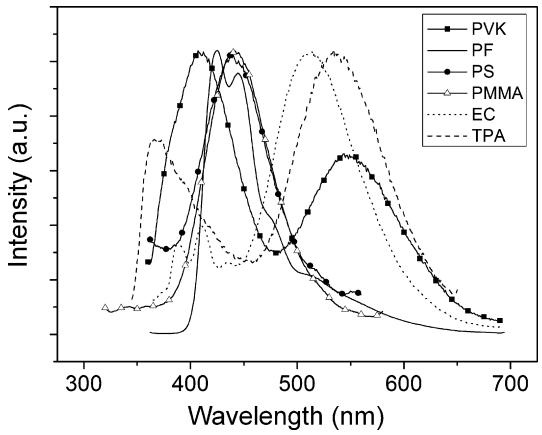

Fig. 8. Film PL spectra of **2** in various polymer and organic hosts.

the N-containing host like PVK which acts as a weak electron-donor and the carborane complex as a weak electron-acceptor due to the presence of electron deficient metal center.

2.3. Luminescent and electron-transporting properties of double-ansa complex 4

In contrast to the non-centrosymmetric **1**, **2** and **3** complexes, the ML was not observed for the double-*ansa* complex **4** owing to the centrosymmetric nature. This result indicates that a sufficient energy is not created to excite molecules in the crystal fractures probably due to an offset of dipole moment in the centrosymmetric unit cell [4].

The absorption and emission spectra of **4** in solution and solid state are shown in Fig. 9. While the chloroform solution of **4** shows a distinct low-energy absorption band at 416 nm, the absorption is largely red-shifted in comparison with that of the non-centrosymmetric zirconium complex **2** (λ_{abs} = 290 nm). Similarly, the emission band at 544 nm with a moderate shoulder around 500 nm is also red-shifted (λ_{em} = 441 nm for **2**). These results are indicative of the reduced LMCT transition energy in **4**, and thus it might suggest that the LUMO contributed mainly by the d^0 Zr center is stabilized by the electron-withdrawing chlorine atom. The solid state PL spectrum also displays an emission band with a similar peak position (λ_{em} = 549 nm) in the solution PL, but the much increased emission intensity is observed.

Although an OLED device was fabricated by vacuum deposition of the double-*ansa* Zr complex **4** as emitting materials in order to evaluate a potentiality of **4** in the OLED applications, the emission of the deposited film of **4** was quenched quickly. Instead, **4** was further investigated as electron-transporting layer (ETL) materials in OLED since the HOMO–LUMO energy levels of **4** calculated from the optical band gap and oxidation onset potential measured by the UV–Vis absorption and cyclic voltammetry are found to be 5.6 and 2.9 eV, respectively, comparable to those of the well-known ETL materials such as Alq_3 (5.8 and 3.1 eV) [20].

Two OLED structures (OLED-**4** and OLED-Alq_3) are thus constructed as follows: ITO (anode)/*m*-MTDATA (HIL, 60 nm)/α-NPD (HTL, 20 nm)/Alq_3 (EML, 30 nm)/**4** or Alq_3 (ETL, 30 nm)/LiF (EIL, 1 nm)/Al (cathode, 100 nm) (*m*-MTDATA = 4,4′,4″-tris(*N*-3-methylphenyl-*N*-phenylamino)-triphenylamine, HIL = hole-injection layer, α-NPD = 4,4′-bis(*N*-1-naphthyl-*N*-phenylamino)biphenyl, HTL = hole-transporting layer, Alq_3 = tris(8-hydroxyquinolinolato)aluminum, EIL = electron-injection layer). Both devices displayed almost identical EL spectra with 520-nm green emission of Alq_3 (Fig. 10), thus indicating that **4** functions properly as ETL materials. The CIE color coordinate of OLED-**4** is only slightly changed from (0.31, 0.53) at 10 mA cm^{-2} to (0.30, 0.53) at 100 mA cm^{-2}, while OLED-Alq_3 maintained the constant CIE coordinate of (0.31, 0.52) at both current densities.

According to the current density vs. voltage and luminance vs. current density characteristics of OLED-**4** and OLED-Alq_3 displayed

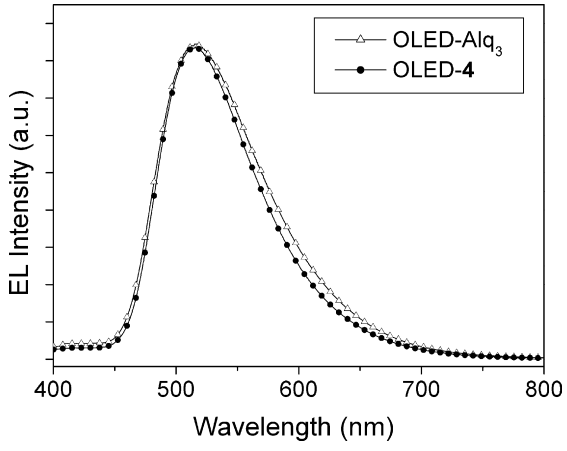

Fig. 10. EL spectra of devices incorporating Alq_3 and **4** as ETL, respectively.

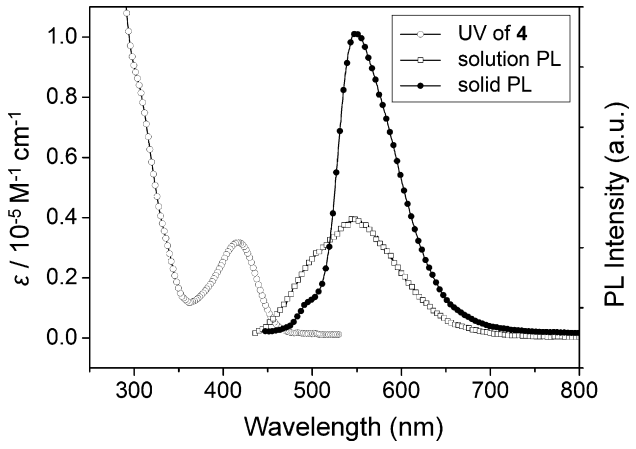

Fig. 9. UV–Vis and PL (solid and solution) spectra of **4**.

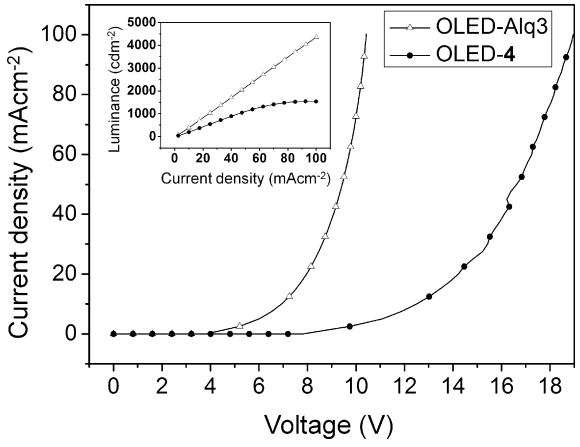

Fig. 11. Current density vs. voltage characteristics of devices incorporating Alq_3 and **4** as ETL, respectively. Inset: Luminance vs. current density characteristics of the devices.

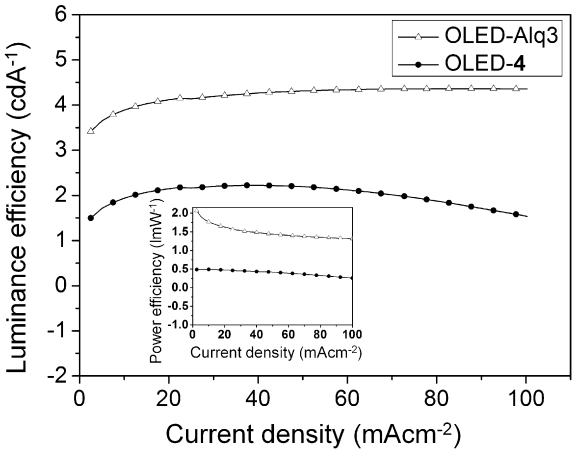

Fig. 12. Luminance efficiency vs. current density characteristics of devices incorporating Alq_3 and **4** as ETL, respectively. Inset: Power efficiency vs. current density characteristics of the devices.

in Fig. 11, the low turn-on voltages of 3.2 V and 2.6 V, respectively, are observed. However, with increasing applied voltage, both the current density and luminance of OLED-Alq_3 increase much faster than those of OLED-**4**. For instance, the driving voltage at a current density of 50 mA cm^{-2} is 9.4 V for OLED-Alq_3 while that for OLED-**4** is 16.6 V. Nevertheless, the luminance of 1100 cd m^{-2} for OLED-**4** at 50 mA cm^{-2} is half the level obtained for OLED-Alq_3 (2200 cd m^{-2}). As shown in Fig. 12, the luminance efficiency and power efficiency of 2.2 cd A^{-1} and 0.42 lm W^{-1}at 50 mA cm^{-2}, respectively, for OLED-**4** are also reasonably high although they are lower than those for OLED-Alq_3 (4.3 cd A^{-1} and 1.4 lm W^{-1} at 50 mA cm^{-2}, respectively). Despite the overall lower performance in comparison with that of OLED-Alq_3, these results indicate that the complex **4** is able to act as electron-transporting materials in OLEDs, suggesting a good electron accepting and donating ability of **4** due to the presence of *o*-carborane.

3. Conclusion

We have demonstrated the novel luminescent properties of group 4 complexes derived from *o*-carborane. The non-centrosymmetric crystals of Zr and Hf complexes **2** and **3** induced blue mechanoluminescence (ML) and photoluminescence (PL), but the Ti congener **1** did not show ML and afforded very low PL quantum yield. When doped with PVK host, **2** and **3** also gave rise to green electroluminescence (EL), which turned out to be originated from the exciplexes formed with the N-containing host. Although the ML of C_1 symmetric double *ansa*-zirconium complex **4** is lacking owing to the centrosymmetric nature as evidenced by its crystal structure, it exhibited good electron-transporting properties when incorporated into the ETL of Alq_3-based OLEDs, suggesting the involvement of electron donating and accepting ability of an *o*-carboranyl moiety.

4. Experimental

All operations were performed under an inert nitrogen atmosphere using standard Schlenk and glove box techniques. Anhydrous grade solvents were purified by passing through an activated alumina column. All solvents were stored over activated molecular sieves (5 Å). All starting materials were used without any further purification after purchasing from Aldrich except for *o*-carborane (KatChem). ^1H and ^{13}C NMR spectra were recorded on Bruker AM 300 and Bruker Avance 400 spectrometers at ambient temperature. Elemental analyses were carried out on a Carlo Erba EA 1108 at Korea Basic Science Center (KBSC). UV–Vis spectra were measured using a Jasco V-530 spectrophotometer. PL spectra were measured with a Spex Fluorog-3 luminescence spectrometer. $TiCl_4(thf)_2$ and quinine sulfate were purchased from Strem and Fluka, respectively. Polymeric and organic hosts for PL studies were purchased from Aldrich (poly(9-vinylcarbazole) (PVK), polystyrene (PS), poly(methyl methacrylate) (PMMA), 9-ethylcarbazole (EC) and triphenylamine (TPA)). Polyfluorene (PF) was prepared according to the known procedure [21]. PL quantum yields of the complexes were determined relative to 1.0×10^{-5} quinine sulfate in 1 N H_2SO_4 solution ($\eta = 0.55$) [22]. The compounds, $CpHCMe_2CB_{10}H_{10}CH$ (**I**) [5], 1-(Chlorodimethylsilyl)indene ($Me_2Si(HInd)Cl$) [8], and $M(\eta^5{:}\eta^1\text{-}CpCMe_2CB_{10}H_{10}C)_2$ (M = Zr; **2** [5] and Hf; **3** [4]) were prepared according to our reported procedures.

4.1. Synthesis of $Ti(\eta^5{:}\eta^1\text{-}CpCMe_2CB_{10}H_{10}C)_2$ (**1**)

Compound **1** was prepared according to a procedure analogous to its zirconium [5] and hafnium [4] congeners. Pre-cooled (−78 °C) toluene (40 mL) was added to a solid mixture of $Li_2(\eta^5{:}\eta^1\text{-}CpCMe_2CB_{10}H_{10}C)$ [5] (1.1 g, 4.0 mmol) and $TiCl_4(thf)_2$ (0.67 g, 2.0 mmol). The resulting reaction mixture was stirred at room temperature for 1 d. The volume of the dark red mixture was reduced to about half and then Et_2O (30 mL) was added. Filtration of the resulting mixture afforded the crude orange solids, which was successively washed with cold toluene (10 mL) and MeOH (10 mL). Drying in vacuo followed by recrystallization from THF/Et_2O gave the pure product **1** (yield 65%). ^1H NMR (300.13 MHz, [D_8]THF): δ 6.85 (dd, J = 5.2, 2.3 Hz, 1H; Cp(*H*)), 6.62 (dd, J = 5.0, 1.9 Hz, 1H; Cp(*H*)), 6.30 (dd, J = 5.0, 2.1 Hz, 1H; Cp(*H*)), 5.90 (dd, J = 4.9, 2.7 Hz, 1H; Cp(*H*)), 1.72 (s, 3H; $C(CH_3)_2$), 1.44 (s, 3H; $C(CH_3)_2$); $^{13}C\{^1H\}$ NMR (75.475 MHz, [D_8]THF): δ 162.36 (Cp(*C*)C), 122.74 (Cp(*C*)H), 119.64 (Cp(*C*)H), 114.44 (Cp(*C*)H), 112.37(Cp(*C*)H), 111.24 ($CB_{10}C$), 106.80 ($CB_{10}C$), 42.16 ($C(CH_3)_2$), 32.63 ($C(CH_3)_2$), 31.85 ($C(CH_3)_2$); $^{11}B\{^1H\}$ NMR (96.275 MHz, [D_8]THF): δ 2.54 (br, 2B), 4.71 (br, 2B), 7.36 (br, 4B), 9.60 (br, 2B); IR (KBr, cm^1): ν (BH) = 2635 (s), 2614 (vs), 2566 (vs), 2537 (vs); Anal. Calc. for $C_{20}H_{40}B_{20}Ti$: C, 43.94; H, 7.74. Found: C, 44.11; H, 7.40.

4.2. Synthesis of $Me_2Si(HInd)(HCp\text{-}3\text{-}(CMe_2CB_{10}H_{10}CH))$ (**II**)

To a cooled (−78 °C) solution of $Me_2Si(HInd)Cl$ (4.2 g, 20 mmol) in Et_2O (20 mL) was added one equiv of a pre-cooled Et_2O solution of lithium salt of **I** (5.1 g, 20 mmol). The reaction mixture was allowed slowly to warm to room temperature and stirred at room temperature. After stirring for 1 d, an aqueous NH_4Cl solution was added and the organic layer was collected by extraction with Et_2O. Removal of the solvent under reduced pressure gave orange sticky solid, which was purified by column chromatography (eluent: CH_2Cl_2/*n*-hexane = 1:10) to yield **II** as a pale yellow sticky oil (3.8 g, 45%). The product was a mixture of stereoisomers, with the major isomer having the following spectroscopic data. ^1H NMR (300.13 MHz, $CDCl_3$, ppm): δ 7.43–7.53 (m, 2H; Ind(*H*)), 7.28–7.30 (m, 1H; Ind(*H*)), 7.21–7.22 (m, 1H; Ind(*H*)), 7.01 (d, 1H; Ind(*H*)), 6.69 (br s, 1H; Ind(*H*)), 6.05–6.51 (m, 3H; Cp(*H*)), 3.59 (s, 1H; SiInd*H*), 3.08 (br, 1H; $CB_{10}CH$), 3.02 (m, 1H; SiCp*H*), 1.55 (s, 6H; $C(CH_3)_2$), −0.05 (s, 3H; $Si(CH_3)_2$), −0.21 (s, 3H; $Si(CH_3)_2$). $^{11}B\{^1H\}$ NMR (96.275 MHz, $CDCl_3$, ppm): −4.43 (br, 2B), −9.27 (br, 2B), −11.79 (br, 2B), −14.03 (br, 4B). ESI-MS: m/z = 483.

4.3. Synthesis of $Me_2Si(\eta^5\text{-}Ind)[\eta^5{:}\eta^1\text{-}Cp\text{-}3\text{-}(CMe_2CB_{10}H_{10}C)]ZrCl$ (**4**)

A solution of $Zr(NMe_2)_4$ (0.59 g, 2.2 mmol) in *n*-hexane was added to a cold (−78 °C) solution of **II** (0.94 g, 2.2 mmol) in

n-hexane under N_2 atmosphere. The reaction flask was allowed slowly to warm to room temperature and then heated to reflux for 1 day. The red–orange reaction mixture was cooled to room temperature and then treated with an excess amount of Me_3SiCl (0.84 ml, 6.6 mmol). The reaction mixture was heated to reflux for 12 h. The yellow solid formed was obtained by filtration. Recrystallization from a THF/*n*-hexane solution at −20 °C afforded yellow crystals of **4** in 85% yield. ^{1}H NMR(400.13 MHz, $CDCl_3$, ppm): δ 7.74 (d, J = 8.6 Hz, 1H; Ind(*H*)), 7.48 (t, J = 6.0 Hz, 1H; Ind(*H*)), 7.33 (d, J = 8.6 Hz, 1 H; Ind(*H*)), 7.25 (d, J = 3.7 Hz, 1H, Ind(*H*)), 7.12 (t, J = 6.8 Hz, 1H; Ind(*H*)), 6.66 (t, J = 2.5 Hz, 1H; Ind(*H*)), 5.78 (d, J = 3.2 Hz, 1H; Cp(*H*)), 5.62 (t, J = 2.4 Hz, 1H; Cp(*H*)), 5.50 (t, J = 2.8 Hz, 1H; Cp(*H*)), 1.57 (s, 3H; $C(CH_3)_2$), 1.54 (s, 3H; $C(CH_3)_2$), 0.96 (s, 3H; $Si(CH_3)_2$), 0.83 (s, 3H; $Si(CH_3)_2$). ^{13}C NMR (100.62 MHz, $CDCl_3$, ppm): δ 157.75 (Cp(*C*)C), 134.45 (Ind(*C*)H), 129.85 (Ind(*C*)H), 128.12 (Ind(*C*)H, 2C), 126.83 (Ind(*C*)H), 123.69 (Ind(*C*)H), 122.64 (Ind(*C*)H), 121.84 (Ind(*C*)H), 116.68 (Cp(*C*)H), 111.92 (Cp(*C*)H), 110.82 (Cp(*C*)H), 106.10 (Ind(*C*)Si), 104.58 (Cp(*C*)Si), 104.13 ($CB_{10}C$), 84.90 ($CB_{10}C$), 42.04 ($C(CH_3)_2$), 33.61 ($C(CH_3)_2$), 30.57 ($C(CH_3)_2$), −3.42 ($Si(CH_3)_2$), −3.75 ($Si(CH_3)_2$). ^{11}B{^{1}H} NMR (96.275 MHz, $CDCl_3$, ppm): −3.06 (br, 2B), −6.29 (br, 2B), −8.69 (br, 4B), −11.45 (br, 2B). ESI-MS: m/z = 546. Anal. Calc. for $C_{21}H_{31}B_{10}ClSiZr$: C, 46.17; H, 5.72. Found: C, 45.60; H 5.75.

4.4. X-ray structural determination

The orange single crystals of **1** and yellow crystals of **4** were mounted on a glass fiber at room temperature. The diffraction data were collected on either an Enraf-Nonius CAD4TSB diffractometer (for **1**) or a Bruker Apex II-CCD area detector diffractometer (for **4**) with graphite-monochromated MoKα radiation (λ = 0.71073 Å) at 293(2) K. The structure was solved by direct methods and all non-hydrogen atoms were subjected to anisotropic refinement by full-matrix least-squares on F^2 using the SHELXTL/PC package. Hydrogen atoms were placed at their geometrically calculated positions and refined riding on the corresponding carbon atoms with isotropic thermal parameters. The detailed crystallographic data for **1** and **4** are given in Table 1.

4.5. Measurement of mechanoluminescence (ML)

Pressure was applied to the single crystalline solid samples of the carborane complexes. The resulting emitted light was guided to the spectrograph (Action Research, SP150, f = 15 cm) via optical fiber (800 μm), and the time-integrated emitting spectra were recorded on CCD detector (Princeton Instruments, RTEA-CCD 128) as the ML spectra.

4.6. Measurement of emission lifetime

The third harmonic output (355 nm) of a Nd:YAG laser (Spectra-Physics, GCR-150) was used as a light source. Emission was detected by a photomultiplier tube (Hamamatzu, H-1949-50) and the optical filter that blocks light below 400 nm was used in front of the photomultiplier tube. The emission lifetimes were measured by a 300 MHz digitized oscilloscope (LeCroy 9361).

4.7. Fabrication of electroluminescent (EL) devices

The configuration of the EL device was ITO/emitting layer (EML)/Li:Al. A layer of carborane complex-doped PVK was fabricated by spin-coating method from THF solutions of **2** and **3**. Li:Al cathode was deposited on top of the EML by the vacuum evaporation method at a pressure of 10^{-6} Torr. EL spectra were obtained with a Minolta CS-1000. Current–voltage and luminance-voltage characteristics were recorded on a current–voltage source (Keithley 238) and a luminescence detector (Minolta LS-100). All EL measurements were carried out at room temperature under ambient atmosphere.

Acknowledgment

We gratefully acknowledge the Korea Science and Engineering Foundation (R01-2007-000-20299-0) for financial support.

Appendix A. Supplementary material

CCDC 702731 and 702732 contain the supplementary crystallographic data for **1** and **4**. These data can be obtained free of charge via www.ccdc.cam.ac.uk/conts/retrieving.html. Supplementary data associated with this article can be found, in the online version, at doi:10.1016/j.jorganchem.2008.12.062.

References

[1] (a) C.W. Tang, S.A. VanSlyke, Appl. Phys. Lett. 51 (1987) 913;
(b) U. Mitschke, P. Bäuerle, J. Mater. Chem. 10 (2000) 1471;
(c) L.S. Hung, C.H. Chen, Mater. Sci. Eng. Res. 39 (2002) 143.
[2] (a) M. Hissler, J.E. McGarrah, W.B. Connick, D.K. Geiger, S.D. Cummings, R. Eisenberg, Coord. Chem. Rev. 208 (2000) 115;
(b) K.-J. Jiang, N. Masaki, J.-B. Xia, S. Noda, S. Yanagida, Chem. Commun. (2006) 2460;
(c) M.S. Rodríguez-Morgade, T. Torres, C. Atienza-Castellanos, D.M. Guldi, J. Am. Chem. Soc. 128 (2006) 15145.
[3] (a) E. Cariati, J. Bourassa, P.C. Ford, Chem. Commun. (1998) 1623;
(b) R. Gao, D.G. Ho, B. Hernandez, M. Selke, D. Murphy, P.I. Djurovich, M.E. Thompson, J. Am. Chem. Soc. 124 (2002) 14828;
(c) I.H.A. Badr, M.E. Meyerhoff, J. Am. Chem. Soc. 127 (2005) 5318.
[4] E. Hong, H. Jang, Y. Kim, S.C. Jeoung, Y. Do, Adv. Mater. 13 (2001) 1094.
[5] E. Hong, Y. Kim, Y. Do, Organometallics 17 (1998) 2933.
[6] H. Kunkely, A. Vogler, Inorg. Chim. Acta 357 (2004) 4607.
[7] (a) J.I. Zink, Acc. Chem. Res. 11 (1978) 289;
(b) B.P. Chandra, D.R. Vij (Eds.), Luminescence of Solids, Plenum Press, New York, 1998, p. 361;
(c) L.M. Sweeting, Chem. Mater. 13 (2001) 854;
(d) I. Sage, G. Bourhill, J. Mater. Chem. 11 (2001) 231.
[8] W. Song, K. Shackett, J.C.W. Chien, M.D. Rausch, J. Organomet. Chem. 501 (1995) 375.
[9] (a) H. Wang, H.-W. Li, X. Huang, Z. Lin, Z. Xie, Angew. Chem., Int. Ed. 42 (2003) 4347;
(b) Y. Wang, H. Wang, H. Wang, H.-S. Chan, Z. Xie, J. Organomet. Chem. 683 (2003) 39;
(c) H. Wang, Y. Wang, H.-W. Li, Z. Xie, Organometallics 20 (2001) 5110.
[10] (a) D.J. Cardin, M.F. Lappert, C.L. Raston, Chemistry of Organo-Zirconium and -Hafnium Compounds, Wiley, New York, 1986;
(b) T.N. Doman, T.K. Hollis, B. Bosnich, J. Am. Chem. Soc. 117 (1995) 1352.
[11] W.J. Gauthier, J.F. Corrigan, N.J. Taylor, S. Collins, Macromolecules 28 (1995) 3771.
[12] (a) G.E. Hardy, J.C. Baldwin, J.I. Zink, W.C. Kaska, P.-H. Liu, L. Dubois, J. Am. Chem. Soc. 99 (1977) 3552;
(b) B.P. Chandra, M. Elyas, K.K. Shrivastava, R.D. Verma, Solid State Commun. 36 (1980) 931.
[13] J.P. Duignan, I.D.H. Oswald, I.C. Sage, L.M. Sweeting, K. Tanaka, T. Ishihara, K. Hirao, G. Bourhill, J. Lumin. 97 (2002) 115.
[14] (a) L.M. Sweeting, A.L. Rheingold, J.M. Gingerich, A.W. Rutter, R.A. Specne, C.D. Cox, T.J. Kim, Chem. Mater. 9 (1997) 1103;
(b) E. Leyrer, F. Zimmerman, J.I. Zink, G. Gliemann, Inorg. Chem. 24 (1985) 102;
(c) G.N. Chapman, A.J. Walton, J. Phys. C: Solid State Phys. 16 (1983) 5543;
(d) G.E. Hardy, B.P. Chandra, J.I. Zink, A.W. Adamson, R.C. Fukuda, R.T. Walters, J. Am. Chem. Soc. 101 (1979) 2787.
[15] (a) G.V. Loukova, V.A. Smirnov, Chem. Phys. Lett. 329 (2000) 437;
(b) V. W.-W. Yam, G.-Z. Qi, K.-K. Cheung, Organometallics 17 (1998) 5448.
[16] J.W. Kenney, D.R. Boone, D.R. Striplin, Y.-H. Chen, K.B. Hamar, Organometallics 12 (1993) 3671.
[17] (a) M. Pope, C.E. Swenberg (Eds.), Electronic Processes in Organic Crystals and Polymers, Oxford University Press, New York, 1999, p. 739;
(b) M. Cocchi, D. Virgili, G. Giro, V. Fattori, P.D. Marco, J. Kalinowski, Y. Shirota, Appl. Phys. Lett. 80 (2002) 2401;
(c) W.M. Su, W.L. Li, Q. Xin, Z.S. Su, B. Chu, D.F. Bi, H. He, J.H. Niu, Appl. Phys. Lett. 91 (2007) 043508/1.
[18] (a) J.-F. Morin, M. Leclerc, D. Adès, A. Siove, Macromol. Rapid Commun. 26 (2005) 761;
(b) J.V. Grazulevicius, P. Strohriegl, J. Pielichowski, K. Pielichowski, Prog. Polym. Sci. 28 (2003) 1297.

[19] (a) D.D. Gebler, Y.Z. Wang, J.W. Blatchford, S.W. Jessen, D.-K. Fu, T.M. Swager, A.G. McDiarmid, A.J. Epstein, Appl. Phys. Lett. 70 (1997) 1644;
(b) G. Giro, M. Cocchi, J. Kalinowski, P. Di, Marco, V. Fattori, Chem. Phys. Lett. 318 (2000) 137;
(c) H. Ogawa, R. Okuda, Y. Shirota, Appl. Phys. A 67 (1998) 599;
(d) L.C. Palilis, A.J. Mäkinen, M. Uchida, Z.H. Kafafi, Appl. Phys. Lett. 82 (2003) 2209.
[20] I.G. Hill, A. Kahn, J. Appl. Phys. 86 (1999) 4515.
[21] M. Kreyenschmidt, G. Klärner, T. Fuhrer, J. Ashenhurst, S. Karg, W.D. Chen, V.Y. Lee, J.C. Scott, R.D. Miller, Macromolecules 31 (1998) 1099.
[22] J.N. Demas, G.A. Crosby, J. Phys. Chem. 75 (1971) 991.